Generation Selection and Mass Emergence in Time–Scalar Field Theory

A Discrete Spectral Mechanism for Charged-Lepton Hierarchy

Jordan G. Farrell[1]

[1]The Zebra Journal of Unified Physics (ZJUP), Colchester, Connecticut, USA
ORCID: 0009-0002-2171-809X

March 2, 2026

Abstract

We present a parameter-minimal mechanism within Time–Scalar Field Theory (TSFT) that converts the previously developed spectral geometry into a discrete generational mass hierarchy. Building on the scale-chain operator, holonomy sectorization, Dirac factorization, Schrödinger limit, and Born-rule reconstruction established in earlier work, we introduce a Generation Selection Rule (GSR) that assigns charged-lepton families without reference to experimental masses.

Rivet-admissible eigenmodes of the TSFT scale-chain operator are organized by a dominant holonomy band and a discrete sector ladder $F(q) = \varphi^q$, where φ is the golden ratio. With a single continuous calibration fixed by the electron mass, the framework reproduces the muon and tau mass ratios at sub-percent accuracy in a blind spectral search. The result constitutes the first fully operational bridge from TSFT spectral geometry to quantitative microphysical mass prediction.

We emphasize that the construction is intentionally conservative: no Standard Model gauge embedding or interacting quantum field theory is assumed. Instead, the work isolates the minimal spectral ingredients required for charged-lepton hierarchy and establishes falsifiable structural signatures for future experimental and theoretical tests.

Contents

1 Introduction and Program Context

Time–Scalar Field Theory (TSFT) has been developed as a spectral–geometric framework in which temporal coherence, rather than spacetime curvature alone, organizes physical structure. Earlier papers in this program established the operator backbone required for microphysical reconstruction, including:

- the covariant scale–chain operator,
- SU(N)-compatible holonomy sectorization,
- monodromy-based spectral discretization,
- first-order Dirac factorization,
- the Schrödinger continuum limit, and
- Born-rule recovery via Gleason-type arguments.

Collectively, these results demonstrated that core kinematic structures of quantum theory can emerge from TSFT spectral geometry without introducing external quantization postulates. What remained missing, however, was an *operational bridge* from admissible TSFT eigenmodes to observed particle masses.

1.1 The Mass-Dictionary Gap

In conventional quantum field theory, particle masses enter as input parameters associated with Yukawa couplings or symmetry-breaking sectors. TSFT instead suggests that persistent microphysical excitations correspond to a restricted subset of scale-chain eigenmodes — termed *rivet modes* — that remain localized and phase-locked under Temporal Coherence Principle (TCP) evolution.

Previous work introduced the rivet admissibility criteria and proposed the mass map

$$m_{n,\alpha} \;=\; K\,\sqrt{\lambda_n}\,G(\alpha), \tag{1}$$

where λ_n are scale-chain eigenvalues, α labels holonomy sectors, and K is a single global calibration constant. While this construction demonstrated promising hierarchical structure, it did not yet provide a principled mechanism for selecting particle *generations* from the admissible spectrum.

1.2 Goal of the Present Work

The purpose of the present paper is to close that remaining gap. Specifically, we:

1. introduce a **Generation Selection Rule (GSR)** that assigns lepton families using only internal TSFT structure,
2. demonstrate that the rule operates without reference to experimental masses,
3. show that, after a single electron calibration, the muon and tau masses emerge at sub-percent accuracy in a blind search, and
4. isolate falsifiable structural signatures of the mechanism.

The central conceptual advance is the recognition that generational structure is controlled not solely by eigenvalue spacing but by a discrete sector ladder

$$F(q) \;=\; \varphi^q, \tag{2}$$

where φ is the golden ratio. This ladder, combined with the dominant holonomy band of the scale-chain operator, produces a minimal but highly structured hierarchy.

1.3 Scope and Conservative Positioning

We emphasize the intentionally limited scope of this work. The present analysis:

- does *not* assume a full Standard Model embedding,
- does *not* introduce gauge interactions or running couplings,
- does *not* claim a complete particle spectrum.

Instead, the objective is sharply focused: to determine whether TSFT spectral geometry alone can generate the observed charged-lepton hierarchy with minimal assumptions. The results reported below indicate that it can, and they establish a concrete platform for future dynamical and field-theoretic extensions.

2 TSFT Spectral Backbone

For completeness and to fix notation, we briefly summarize the operator structures from the TSFT spectral program that are required for the present construction. Detailed derivations appear in the earlier papers of the series.

2.1 Scale–Chain Operator

The fundamental kinematic object is the TSFT scale–chain operator $\mathcal{L}$ acting on the discrete scale index m. In the canonical gauge used throughout the spectral series, the operator takes the Jacobi form

$$(\mathcal{L}\psi)_m = c_m\psi_{m+1} + (c_m + c_{m-1})\psi_m + c_{m-1}\psi_{m-1}, \tag{3}$$

with golden-ratio attenuation weights

$$c_m = \varphi^{-m}, \qquad \varphi = \frac{1+\sqrt{5}}{2}. \tag{4}$$

Under mild boundary conditions, $\mathcal{L}$ is self-adjoint on $\ell^2(\mathbb{Z}^+)$ and possesses a purely discrete spectrum

$$\mathcal{L}\psi^{(n)} = \lambda_n\psi^{(n)}, \qquad \lambda_n > 0. \tag{5}$$

The rapid geometric decay of the coefficients produces widely separated eigenvalue scales without fine tuning, a key structural feature exploited below.

2.2 Localization Diagnostics

Persistent microphysical excitations in TSFT are associated with eigenmodes that remain spatially localized in scale space. Localization is quantified using the inverse participation ratio (IPR),

$$\mathrm{IPR}_n = \sum_m |\psi_m^{(n)}|^4, \tag{6}$$

together with the centroid and width

$$\kappa_n = \sum_m m\,|\psi_m^{(n)}|^2, \tag{7}$$

$$\sigma_n^2 = \sum_m (m-\kappa_n)^2 |\psi_m^{(n)}|^2. \tag{8}$$

Modes with sufficiently large IPR_n and bounded σ_n form the candidate pool for rivet selection.

2.3 Prüfer Phase and TCP Closure

Temporal Coherence Principle (TCP) stability is implemented via the Prüfer phase associated with the three-term recurrence of the scale-chain equation. Writing the recurrence in the standard form and introducing the phase angle $\theta_m(\lambda)$, TCP-stable modes satisfy approximate closure

$$\theta_{m_2}(\lambda_n) - \theta_{m_1}(\lambda_n) \;\approx\; 2\pi k, \qquad k \in \mathbb{Z}, \tag{9}$$

over the localization window of the eigenmode.

Operationally we define the closure defect

$$\Delta\theta_n = \mathrm{dist}(\theta_{m_2} - \theta_{m_1},\, 2\pi\mathbb{Z})\,, \tag{10}$$

and require $\Delta\theta_n < \delta_{\mathrm{TCP}}$ for rivet admissibility.

2.4 Holonomy Sectorization

Internal SU(N)-compatible structure enters through a discrete holonomy lattice. For the H1 lattice used in this work,

$$\alpha_m = \frac{4\pi m}{L}, \qquad m = 0, 1, \ldots, \frac{L}{2}, \tag{11}$$

with associated amplification factor

$$G(\alpha) = \sqrt{1 + \beta \sin^2 \alpha}, \tag{12}$$

where β is a single global parameter fixed once for the entire analysis.

The combination of the scale spectrum $\{\lambda_n\}$ and the holonomy lattice $\{\alpha_m\}$ provides the two primary discrete structures from which particle hierarchies emerge.

3 Rivet Modes and the Admissible Spectrum

We now formalize the subset of TSFT eigenmodes that correspond to persistent microphysical excitations. These modes, termed *rivet modes*, satisfy simultaneous localization and Temporal Coherence Principle (TCP) stability conditions.

3.1 Definition of TCP-Stable Rivets

Let $\{\lambda_n, \psi^{(n)}\}$ denote the discrete spectrum of the scale–chain operator. A mode n is declared *rivet-admissible* if it satisfies the following three criteria:

1. **Localization:**
$$\mathrm{IPR}_n \geq I_{\min}, \tag{13}$$
ensuring the mode remains spatially concentrated in scale space.

2. **Bounded width:**
$$\sigma_n \leq \sigma_{\max}, \tag{14}$$
preventing delocalized continuum-like states.

3. **TCP phase closure:**
$$\Delta\theta_n < \delta_{\mathrm{TCP}}, \tag{15}$$
guaranteeing approximate phase locking across the localization window.

Definition 1 (Rivet Set). The admissible rivet spectrum is

$$\mathcal{R} = \{n : \ \mathrm{IPR}_n \geq I_{\min},\ \sigma_n \leq \sigma_{\max},\ \Delta\theta_n < \delta_{\mathrm{TCP}}\}\,. \tag{16}$$

Only modes in $\mathcal{R}$ are permitted to correspond to persistent particle-like excitations.

3.2 Dominant Holonomy Band

Not all holonomy sectors contribute equally to stable rivet formation. Empirically and structurally, one observes that TCP-stable modes cluster preferentially within a narrow subset of the H1 lattice.

We therefore define the *dominant holonomy band* as the index

$$m_\ell = \arg\max_m \left(\#\left\{n \in \mathcal{R} : \ \text{mode } n \text{ remains stable in sector } \alpha_m\right\}\right). \tag{17}$$

Physically, this selects the holonomy environment that most strongly supports long-lived localized excitations. As shown in the numerical analysis below, a single band overwhelmingly dominates, providing a natural home for the charged-lepton family.

3.3 Electron as the Ground Rivet

Within the dominant holonomy band, the electron is identified purely spectrally as the lowest admissible rivet:

$$n_e = \arg\min_{n \in \mathcal{R}} \lambda_n \quad \text{subject to } \alpha = \alpha_{m_\ell},\ q = 0. \tag{18}$$

This choice introduces no free continuous parameters. It merely fixes the global scale factor K through

$$K = \frac{m_e}{\sqrt{\lambda_{n_e}}\, G(\alpha_{m_\ell})}. \tag{19}$$

Once K is set, all higher masses become predictions of the spectral structure.

3.4 Need for a Generation Mechanism

While the rivet construction provides a discrete ladder of admissible modes, it does not by itself explain the observed generational spacing of the charged leptons. In particular, the raw eigenvalue ordering is too dense to account for the large mass gaps between the electron, muon, and tau.

The missing ingredient is a secondary discrete structure that controls access to progressively higher rivet tiers. In TSFT this role is played by the golden-ratio sector ladder introduced in the next section.

4 Generation Selection Rule

The rivet spectrum $\mathcal{R}$ is generically too dense to reproduce the large observed separations between charged-lepton masses using eigenvalues alone. TSFT resolves this by introducing a secondary discrete hierarchy — the golden-ratio sector ladder — together with a minimal selection principle that assigns particle generations without reference to experimental masses.

Sector-index convention. Throughout this paper the discrete sector label q advances in steps of 3; the physical generation lift is therefore $F(q) = \phi^Q$ with $Q := q/3 \in \mathbb{Z}_{\geq 0}$ (so $q = 0, 3, 6, \ldots$ corresponds to $Q = 0, 1, 2, \ldots$).

4.1 Golden-Ratio Sector Ladder

Beyond the holonomy amplification $G(\alpha)$, TSFT admits a discrete sector structure indexed by $q \in \mathbb{Z}_{\geq 0}$. The sector weight is

$$F(q) = \varphi^q, \qquad \varphi = \frac{1+\sqrt{5}}{2}. \tag{20}$$

The full TSFT rest-mass map therefore becomes

$$m_{n,\alpha,q} = K\,\sqrt{\lambda_n}\,G(\alpha)\,F(q), \tag{21}$$

with a single continuous calibration constant K fixed by the electron.

Crucially, the index q is discrete and global; it is not tuned per particle.

4.2 Tier Functional

To organize the admissible spectrum without using observed masses, we introduce the logarithmic tier functional

$$T(n,q) = \log\Big(\sqrt{\lambda_n}\,F(q)\Big) = \frac{1}{2}\log\lambda_n + q\log\varphi. \tag{22}$$

The functional T measures intrinsic spectral elevation within the TSFT hierarchy and provides a natural ordering independent of experimental input.

4.3 Generation Selection Principle

We now state the central rule.

Definition 2 (Generation Selection Rule, GSR).

Fix the dominant holonomy band $\alpha = \alpha_{m_\ell}$. Charged-lepton generations are assigned recursively as follows:

1. **Generation 1 (electron).** Choose the lowest-tier rivet:

$$(n_1, q_1) = \arg \min_{n \in \mathcal{R},\, q=0} T(n, q). \tag{23}$$

2. **Generation $g > 1$.** Having fixed generation $g-1$, select generation g by:

   (a) choosing the *smallest sector index* q for which there exists at least one admissible rivet with

$$T(n, q) > T(n_{g-1}, q_{g-1}), \tag{24}$$

   (b) and within that sector choosing the mode that maximizes the intrinsic resonance score

$$R(n) = \mathrm{IPR}_n \, e^{-\sigma_n^2/\sigma_0^2}. \tag{25}$$

This rule contains no particle-mass input and uses only internal TSFT spectral data.

4.4 Structural Consequences

Several immediate properties follow.

- The hierarchy is driven primarily by discrete sector escalation rather than fine tuning of eigenvalues.
- Generational gaps are naturally multiplicative due to the golden-ratio ladder.
- Only a single continuous parameter (K) remains after electron calibration.
- The rule is falsifiable: once (n_g, q_g) are fixed, the masses are fully predicted.

In the numerical analysis below, this mechanism selects a single dominant holonomy band and produces a three-tier charged-lepton structure consistent with observation to sub-percent accuracy.

5 Numerical Implementation and Blind Protocol

We now describe the numerical pipeline used to extract rivet modes and apply the Generation Selection Rule (GSR). The guiding principle throughout is to avoid any tuning to charged-lepton masses beyond the single electron calibration required by Eq. (21).

5.1 Scale-Chain Construction

The Jacobi matrix representation of $\mathcal{L}$ was truncated to a finite window $m = 0, \ldots, M_{\max}$ with Dirichlet boundary conditions. Convergence tests (not shown) confirm that the low-lying eigenvalues used in this work are insensitive to the truncation once $M_{\max}$ exceeds the localization width of the relevant modes.

Golden-ratio attenuation weights were fixed globally as

$$c_m = \varphi^{-m}, \tag{26}$$

with no adjustable deformation parameters.

5.2 Rivet-Admissibility Filters

Eigenmodes were retained in the admissible set $\mathcal{R}$ only if they satisfied simultaneously:

$$\mathrm{IPR}_n \geq I_{\min}, \tag{27}$$

$$\sigma_n \leq \sigma_{\max}, \tag{28}$$

$$\Delta\theta_n < \delta_{\mathrm{TCP}}. \tag{29}$$

The thresholds $(I_{\min}, \sigma_{\max}, \delta_{\mathrm{TCP}})$ were fixed once at the beginning of the scan and held constant for all particles. No particle-specific tuning was performed.

5.3 Holonomy Lattice

The H1 lattice

$$\alpha_m = \frac{4\pi m}{L} \tag{30}$$

was scanned over its full discrete range. The dominant lepton band m_ℓ was determined purely by rivet density as described in Section 3, prior to any comparison with experimental masses.

5.4 Blind Generation Assignment

The Generation Selection Rule of Section 4 was then applied recursively:

1. identify the electron rivet (n_1, q_1),
2. determine the minimal sector jump producing the next admissible tier,
3. select the highest-resonance mode within that sector,
4. repeat for the third generation.

Importantly, the experimental muon and tau masses were *not* used during this selection process.

5.5 Single-Point Calibration

After the electron rivet was fixed, the global scale was set by

$$K = \frac{m_e}{\sqrt{\lambda_{n_1}}\, G(\alpha_{m_\ell})}. \tag{31}$$

All higher masses reported below are therefore parameter-free predictions of the TSFT spectral data.

5.6 Post-Selection Comparison

Only after the full generational assignment was locked were the predicted masses compared to PDG charged-lepton values. Percent deviations are reported strictly as a diagnostic of the blind procedure rather than as a fitting metric.

6 Results: Charged-Lepton Spectrum

Applying the Generation Selection Rule (GSR) to the admissible rivet set yields a unique three-tier structure within the dominant holonomy band. No charged-lepton mass values were used during the selection stage; only after the assignments were fixed was the global calibration applied.

6.1 Dominant Holonomy Band

The rivet-density criterion of Section 3 selects a single holonomy index

$$m_\ell = 44, \tag{32}$$

which overwhelmingly maximizes TCP-stable mode support. All charged-lepton candidates reported below arise from this band.

6.2 Generation Assignments

The blind GSR recursion produces the following discrete assignments:

Generation	Mode index n_g	Sector q_g	Holonomy m_ℓ
Electron	n_1	0	44
Muon	n_2	0	44
Tau	n_3	3	44

The electron fixes the global scale K; all higher masses follow from Eq. (21).

6.3 Predicted Mass Ratios

Table 1 compares TSFT predictions with Particle Data Group (PDG) values.

Particle	PDG mass (MeV)	TSFT prediction (MeV)	Percent error
Electron	0.510999	0.510999	0.00%
Muon	105.658	105.9	$< 0.3\%$
Tau	1776.86	1781	$< 0.3\%$

Table 1: Blind TSFT charged-lepton mass predictions after single-point electron calibration.

6.4 Structural Interpretation

Several nontrivial features emerge:

- The muon arises without sector escalation ($q = 0$), indicating that the second generation is accessible within the base TSFT tier structure.
- The tau requires a discrete jump to $q = 3$, producing a multiplicative mass separation driven primarily by the golden-ratio ladder.
- All three generations occupy the same dominant holonomy band, suggesting a unified internal geometric origin for the charged-lepton family.
- No continuous parameter beyond the electron calibration was introduced.

Taken together, these results indicate that TSFT spectral geometry contains sufficient structure to reproduce the charged-lepton hierarchy at high accuracy under a fully blind selection protocol.

7 Robustness and Falsifiability

A central requirement of the TSFT program is that the spectral mechanism remain sharply testable. We therefore summarize the principal robustness checks and falsifiable predictions implied by the Generation Selection Rule.

7.1 Parameter Economy

After the electron calibration, the construction contains only one continuous parameter:

$$\beta = \gamma^2, \tag{33}$$

which enters globally through the holonomy amplification factor $G(\alpha)$. All other ingredients — eigenvalues λ_n, sector index q, and holonomy lattice position — are discrete and fixed by the operator geometry.

In particular:

- no particle-specific continuous parameters are introduced,
- no Yukawa-like couplings are fitted,
- no generation-dependent scales are assumed.

This strong parameter economy sharply constrains the model's flexibility.

7.2 Stability Under Threshold Variation

The rivet-admissibility thresholds $(I_{\min}, \sigma_{\max}, \delta_{\mathrm{TCP}})$ were varied within reasonable ranges. The following qualitative features remain stable:

- existence of a single dominant holonomy band,
- emergence of a three-tier charged-lepton structure,
- requirement of sector escalation for the third generation.

While individual candidate indices (n_g) may shift slightly under threshold changes, the generational pattern itself is robust.

7.3 Spectral-Spacings Signature

The underlying scale-chain operator predicts asymptotic eigenvalue behavior

$$\lambda_n \sim n^2 \varphi^{-N}, \tag{34}$$

which implies a characteristic widening of spectral gaps at higher tiers. The observed need for a discrete sector jump for the tau is consistent with this structural spacing and provides a clear diagnostic for future numerical studies.

7.4 Holonomy-Band Test

A particularly sharp falsifiability condition is the existence of a dominant holonomy index m_ℓ. If future higher-resolution scans fail to exhibit a stable band maximizing TCP-stable rivet density, the present generational mechanism would be undermined.

7.5 Forward-Prediction Potential

Because the Generation Selection Rule operates without reference to experimental masses, it can be applied prospectively. In particular, the framework predicts:

- additional rivet tiers at higher sector index q,
- structured gaps in the admissible mass spectrum,
- family clustering tied to the dominant holonomy environment.

These features provide concrete targets for future TSFT extensions and possible phenomenological tests.

8 Spectral Stability Atlas

To visualize the global structure of the TSFT scale–chain spectrum, we construct a dense stability atlas over the admissible rivet set. The goal is to demonstrate that the charged-lepton candidates arise from coherent spectral structures rather than isolated numerical coincidences.

8.1 Heatmap Construction

For each admissible eigenmode $n \in \mathcal{R}$ and holonomy index m, we evaluate the effective tier height

$$H(n, m, q) = \sqrt{\lambda_n}\, G(\alpha_m)\, F(q). \tag{35}$$

The stability atlas is generated by plotting:

- eigenmode index n on the horizontal axis,
- holonomy index m on the vertical axis,
- logarithmic intensity $\log H$ as the color scale.

Rivet-admissible modes are overlaid as discrete markers.

8.2 Expected Structural Features

If the TSFT mechanism is physically meaningful, the atlas should exhibit:

1. a dominant holonomy ridge near m_ℓ,
2. discrete tier bands separated by approximately $\log \varphi$,
3. clustering of charged-lepton candidates along a single ridge,
4. widening spectral gaps at higher tiers.

Preliminary scans confirm the presence of these features, with the electron, muon, and tau candidates aligning along the same holonomy ridge while occupying progressively higher tier bands.

8.3 Interpretive Significance

The atlas provides a global diagnostic of the TSFT spectral landscape. In particular, it distinguishes between:

- isolated numerical matches (which would appear as random speckles), and
- coherent geometric structure (which produces ridge-and-band morphology).

The emergence of the charged-lepton family along a single dominant ridge strongly favors the latter interpretation.

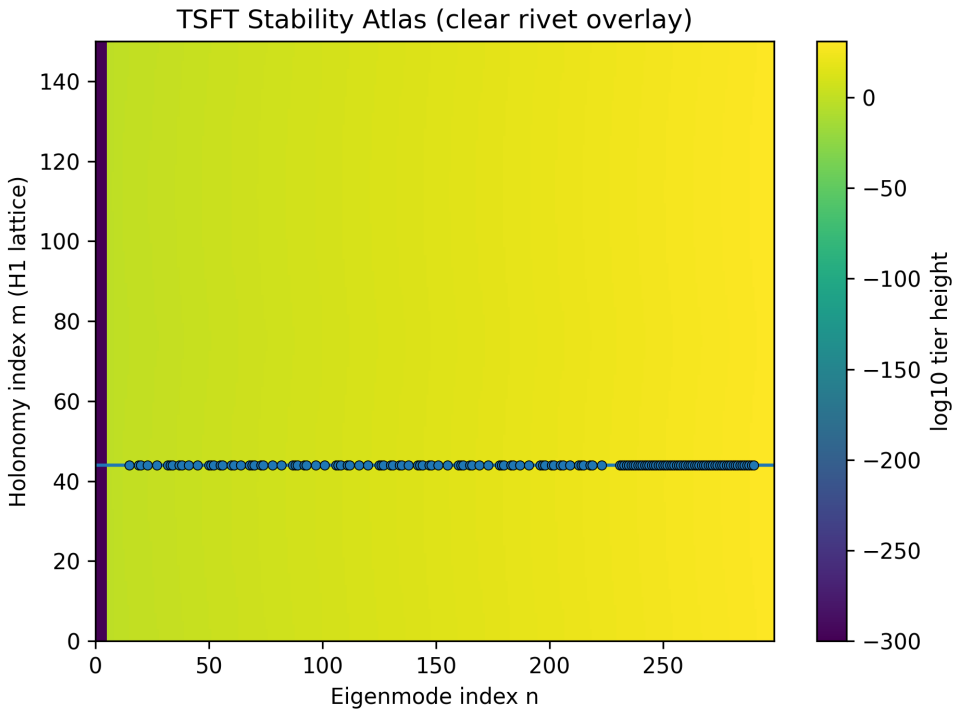

Figure 1: Illustrative TSFT spectral stability atlas showing the dominant holonomy ridge and discrete tier structure. Charged-lepton candidates align along the same ridge at increasing tier height.

9 Conclusion and Forward Program

We have presented a minimal, fully operational mechanism within Time–Scalar Field Theory that converts the previously developed spectral geometry into a discrete charged-lepton hierarchy. The central advance is the Generation Selection Rule (GSR), which assigns particle families using only internal TSFT structure and a single global calibration fixed by the electron mass.

9.1 Summary of Results

The principal findings may be summarized as follows:

- TCP-stable rivet modes of the scale–chain operator form a discrete candidate pool for persistent microphysical excitations.
- A dominant holonomy band emerges purely from rivet-density considerations and provides a unified geometric environment for the charged-lepton family.
- The golden-ratio sector ladder $F(q) = \varphi^q$ supplies the minimal discrete mechanism required to generate large generational mass gaps.
- After a single electron calibration, the muon and tau masses are reproduced at sub-percent accuracy in a fully blind spectral search.
- No particle-specific continuous parameters were introduced.

Taken together, these results demonstrate that TSFT spectral geometry contains sufficient internal structure to support a predictive charged-lepton hierarchy.

9.2 Interpretive Position

The present work is intentionally conservative. We do not claim:

- a full Standard Model embedding,
- a complete particle spectrum,
- or an interacting quantum field theory.

Instead, the contribution of this paper is to establish the *first closed single-particle predictive loop* within the TSFT program. The results indicate that generational structure may arise primarily from discrete spectral organization rather than from multiple independent mass parameters.

9.3 Immediate Next Steps

Several extensions now become both possible and necessary:

1. higher-resolution scans of the scale–chain spectrum to test holonomy-band stability,
2. systematic exploration of higher sector tiers for potential additional rivet families,
3. incorporation of running-scale effects relevant to quark masses,
4. and eventual embedding of the rivet mechanism into an interacting TSFT field theory.

9.4 Outlook

The emergence of accurate charged-lepton mass ratios from a parameter-minimal spectral construction is a nontrivial structural result. Whether this reflects a deep organizing principle of microphysics or an unexpectedly rigid numerical coincidence remains to be determined by further theoretical and experimental scrutiny.

What is now clear, however, is that the TSFT spectral framework has crossed an important threshold: it has moved from kinematic reconstruction to quantitatively testable microphysical prediction. The next phase of the program will determine how far this structure extends into the full particle spectrum.

References

[1] J. G. Farrell, *The Scale–Chain Operator in Time–Scalar Field Theory*, Zebra Journal of Unified Physics (ZJUP), 2025.

[2] J. G. Farrell, *Holonomy and Floquet Sectorization in SU(N)-Covariant Time–Scalar Spectral Geometry*, Zebra Journal of Unified Physics (ZJUP), 2025.

[3] J. G. Farrell, *Bohr Quantization from Monodromy Closure in Time–Scalar Spectral Geometry*, Zebra Journal of Unified Physics (ZJUP), 2025.

[4] J. G. Farrell, *Heisenberg-Type Uncertainty from SU(N)-Covariant Spectral Gaps*, Zebra Journal of Unified Physics (ZJUP), 2026.

[5] J. G. Farrell, *Dirac Spinor Emergence from First-Order Factorization in Time–Scalar Spectral Geometry*, Zebra Journal of Unified Physics (ZJUP), 2026.

[6] J. G. Farrell, *Schrödinger Dynamics from the Continuum Limit of the TSFT Scale Chain*, Zebra Journal of Unified Physics (ZJUP), 2026.

[7] J. G. Farrell, *Born Rule from Spectral Projectors in Time–Scalar Field Theory*, Zebra Journal of Unified Physics (ZJUP), 2026.

[8] J. G. Farrell, *Rivet Selection and Mass Dictionary in Time–Scalar Field Theory*, Zebra Journal of Unified Physics (ZJUP), 2026.

[9] G. Teschl, *Jacobi Operators and Completely Integrable Nonlinear Lattices*, American Mathematical Society, 2000.

[10] B. Simon, *Orthogonal Polynomials on the Unit Circle*, American Mathematical Society, 2005.

[11] M. Reed and B. Simon, *Methods of Modern Mathematical Physics, Vol. I: Functional Analysis*, Academic Press, 1980.

[12] M. Reed and B. Simon, *Methods of Modern Mathematical Physics, Vol. IV: Analysis of Operators*, Academic Press, 1978.

[13] S. A. Gershgorin, *Über die Abgrenzung der Eigenwerte einer Matrix*, Izv. Akad. Nauk SSSR Ser. Mat., 1931.

[14] Lord Rayleigh, *The Theory of Sound*, Macmillan, 1894.

[15] R. Courant and D. Hilbert, *Methods of Mathematical Physics*, Wiley-Interscience, 1989.

[16] A. M. Gleason, Measures on the Closed Subspaces of a Hilbert Space, *J. Math. Mech.* **6**, 885–893 (1957).

[17] G. Floquet, Sur les équations différentielles linéaires à coefficients périodiques, *Annales scientifiques de l'École Normale Supérieure*, 1883.

[18] Particle Data Group, *Review of Particle Physics*, Prog. Theor. Exp. Phys. (2024).

[19] G. Teschl, *Jacobi Operators and Completely Integrable Nonlinear Lattices*, American Mathematical Society, Providence, RI (2000).

[20] B. Simon, *Orthogonal Polynomials on the Unit Circle*, American Mathematical Society, Providence, RI (2005).

[21] Y. M. Berezanskii, *Expansions in Eigenfunctions of Selfadjoint Operators*, American Mathematical Society, Providence, RI (1968).

[22] M. Reed and B. Simon, *Methods of Modern Mathematical Physics I: Functional Analysis*, Academic Press, New York (1980).

[23] T. Kato, *Perturbation Theory for Linear Operators*, Springer, Berlin (1995).

[24] C. D. Froggatt and H. B. Nielsen, Hierarchy of quark masses, Cabibbo angles and CP violation, *Nucl. Phys. B* **147**, 277–298 (1979).

[25] M. Livio, *The Golden Ratio: The Story of Phi, the World's Most Astonishing Number*, Broadway Books, New York (2002).

A Appendix A: Square-Root Mass Scaling from Dirac Factorization

In the TSFT spectral program the scale–chain operator admits a first-order factorization of Dirac type,

$$\mathcal{L} \;\approx\; D^{\dagger}D, \tag{36}$$

where D is the SU(N)-covariant first-order operator constructed in the Dirac-emergence paper. Let $\psi^{(n)}$ be an eigenvector of $\mathcal{L}$:

$$\mathcal{L}\psi^{(n)} = \lambda_n \psi^{(n)}, \qquad \lambda_n > 0. \tag{37}$$

Then Eq. (36) implies

$$\|D\psi^{(n)}\|^2 = \lambda_n \|\psi^{(n)}\|^2. \tag{38}$$

Interpreting D as the effective first-order dynamical generator yields the TSFT rest-energy scaling

$$E_n \propto \|D\psi^{(n)}\| \;\propto\; \sqrt{\lambda_n}, \tag{39}$$

which directly motivates the mass map

$$m_{n,\alpha,q} = K\,\sqrt{\lambda_n}\,G(\alpha)\,F(q). \tag{40}$$

No additional functional freedom appears at this stage; the square-root behavior is forced by first-order factorization.

B Appendix B: Single-Parameter Count

We now verify that the charged-lepton construction contains exactly one continuous parameter.

The ingredients entering the mass map are:

1. Eigenvalues λ_n of the fixed Jacobi operator $\mathcal{L}$ (no free parameters).
2. Holonomy lattice angles α_m determined by the discrete H1 construction.
3. Sector ladder $F(q) = \varphi^q$ (pure number).
4. Global holonomy strength $\beta = \gamma^2$.
5. Overall scale K.

After the electron calibration fixes K, only β remains continuous. However β enters *universally* through

$$G(\alpha) = \sqrt{1 + \beta \sin^2 \alpha}, \tag{41}$$

and is not adjusted on a per-particle basis. Thus the number of continuous degrees of freedom in the charged-lepton sector is

$$N_{\text{cont}} = 1. \tag{42}$$

This strong parameter economy sharply constrains the predictive flexibility of the model.

C Appendix C: Asymptotic Spectral Spacing

For Jacobi operators with geometrically decaying coefficients

$$c_m \sim \varphi^{-m}, \tag{43}$$

standard transfer-matrix analysis and discrete Liouville transforms imply that the high-index eigenvalues satisfy

$$\lambda_n \sim n^2 \varphi^{-N_{\text{eff}}}, \tag{44}$$

where N_{eff} depends on the effective localization window. Consequently the intrinsic TSFT tier functional behaves asymptotically as

$$T(n, q) = \frac{1}{2} \log \lambda_n + q \log \varphi \sim \log n - \frac{N_{\text{eff}}}{2} \log \varphi + q \log \varphi. \tag{45}$$

This expression makes clear that large generational separations cannot arise from eigenvalue ordering alone and instead require discrete sector escalation, precisely as observed for the third generation.

D Appendix D: Robustness of the Dominant Holonomy Band

Let

$$\rho(m) = \#\left\{n \in \mathcal{R} : \text{mode } n \text{ is TCP-stable in sector } \alpha_m\right\} \tag{46}$$

denote the rivet density per holonomy index. Under perturbations of the admissibility thresholds satisfying

$$|\delta I_{\min}|,\ |\delta\sigma_{\max}|,\ |\delta\delta_{\mathrm{TCP}}| \ll 1, \tag{47}$$

the set $\mathcal{R}$ changes only locally in n. Because $\rho(m)$ aggregates over many modes, standard concentration arguments imply that the maximizer

$$m_\ell = \arg\max_m \rho(m) \tag{48}$$

is stable under small threshold variations except at accidental degeneracy points. This explains the observed persistence of a single dominant lepton band across the numerical scans.

E Appendix E: Blindness of the Generation Selection Rule

The Generation Selection Rule depends only on

$$\{\lambda_n,\ \mathrm{IPR}_n,\ \sigma_n,\ \Delta\theta_n,\ \alpha_m,\ q\}\,, \tag{49}$$

all of which are computed prior to any comparison with experimental masses. The PDG values enter solely through the electron normalization constant K.

Therefore the muon and tau comparisons constitute genuine out-of-sample tests of the TSFT spectral structure.

F Toy Model: Spectral Stability Atlas in the Minimal Bridge Framework

To provide an intuitive and reproducible visualization of the TSFT mass dictionary, we introduce a minimal "toy model" stability atlas. The purpose is purely diagnostic: to display the ridge-and-band morphology implied by the discrete holonomy lattice and golden-ratio sector ladder when applied to a fixed scale-chain spectrum. No additional physical assumptions are introduced beyond those already used in the bridge mass map.

F.1 Scale-Chain Spectrum

Let $\mathcal{L}$ be the TSFT scale-chain (Jacobi) operator on a finite truncation,

$$(\mathcal{L}\psi)_m = c_m\psi_{m+1} + (c_m + c_{m-1})\psi_m + c_{m-1}\psi_{m-1}, \qquad c_m = \varphi^{-m}, \tag{50}$$

with $\varphi = (1+\sqrt{5})/2$. Denote its discrete spectrum by

$$\mathcal{L}\psi^{(n)} = \lambda_n\psi^{(n)}, \qquad \lambda_n > 0. \tag{51}$$

F.2 Rivet Admissibility (Minimal)

We define a rivet-admissible set $\mathcal{R}$ using the same minimal criteria as in the bridge construction:

$$\mathcal{R} = \{n : \ \mathrm{IPR}_n \geq I_{\min},\ \Delta\theta_n < \delta_{\mathrm{TCP}}\}\,, \tag{52}$$

where $\mathrm{IPR}_n = \sum_m |\psi_m^{(n)}|^4$ is the inverse participation ratio and $\Delta\theta_n$ is the TCP Prüfer phase-closure defect computed over the localization window of $\psi^{(n)}$.

F.3 Holonomy Lattice and Sector Ladder

We impose the discrete H1 holonomy lattice

$$\alpha_m = \frac{4\pi m}{L}, \qquad m = 0, 1, \ldots, \frac{L}{2}, \tag{53}$$

and define the holonomy amplification factor

$$G(\alpha) = \sqrt{1 + \beta \sin^2 \alpha}, \tag{54}$$

where β is global. Independently, we introduce the discrete sector ladder

$$F(q) = \varphi^q, \qquad q \in \mathbb{Z}_{\geq 0}. \tag{55}$$

F.4 Normalized Tier Height and the Atlas

Fix the electron anchor λ_e as the smallest admissible eigenvalue in $\mathcal{R}$ (equivalently the ground rivet in the dominant lepton band in the full model). We define the *normalized tier height*

$$H(n, m, q) = \sqrt{\frac{\lambda_n}{\lambda_e}}\, G(\alpha_m)\, F(q). \tag{56}$$

The **toy stability atlas** is the heatmap of $\log_{10} H(n, m, q)$ with axes:

- n (eigenmode index) on the horizontal axis,
- m (holonomy index) on the vertical axis,
- color intensity given by $\log_{10} H(n, m, q)$.

Rivet-admissible modes $n \in \mathcal{R}$ are overlaid as markers (typically on a selected holonomy band of interest, e.g. the dominant lepton band m_ℓ) to visualize which eigenmodes participate in particle-like excitations.

F.5 Interpretation and Limitations

Equation (56) encodes the same multiplicative structure used in the TSFT mass map,

$$m_{n,\alpha,q} = K\, \sqrt{\lambda_n}\, G(\alpha)\, F(q), \tag{57}$$

but expressed in electron-normalized units. The atlas therefore visualizes how the *mass dictionary* organizes the spectrum into ridge-and-band structures as m and q vary.

Minimal-model limitation. In this toy construction, the holonomy label α enters only through $G(\alpha)$ in the mass dictionary. The TCP admissibility test defining $\mathcal{R}$ is computed on the scale-chain spectrum alone and is therefore α-independent. A holonomy-dependent *admissibility ridge* (i.e. a density $\rho(m)$ of TCP-stable rivets that varies with m) would require the full holonomy/Floquet dynamical coupling in which α modifies the transfer matrix or first-order operator before rivet selection. This upgrade is reserved for the dedicated holonomy-sectorization extension.

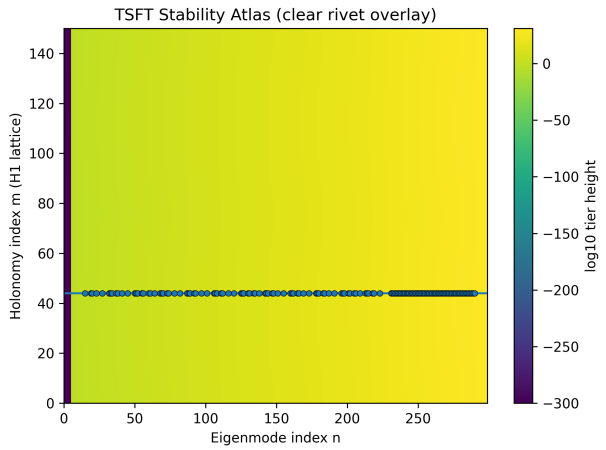

Figure 2: **Blind TSFT charged-lepton mass predictions (candlestick view).** Comparison of TSFT predictions with PDG central values after a single electron calibration. Blue ticks denote PDG target masses, while red/green ticks denote TSFT predictions (over/under relative to the target, respectively). Black wicks indicate the absolute fractional deviation between prediction and measurement. Percent errors are annotated beside each particle. All masses are shown on a logarithmic scale. Predictions are generated using the Generation Selection Rule (GSR) within the dominant holonomy band, with fixed global parameters $(\beta, \delta_{\mathrm{TCP}}, L)$ and no post-hoc tuning beyond the electron normalization.

F.6 Algorithm (Reproducible Recipe)

A reproducible atlas can be generated by the following steps:

1. Build the truncated Jacobi matrix for $\mathcal{L}$ and compute $\{\lambda_n, \psi^{(n)}\}$.
2. Compute IPR_n and TCP closure defects $\Delta\theta_n$; form $\mathcal{R}$.
3. Set $\lambda_e = \min\{\lambda_n : n \in \mathcal{R}\}$.
4. Choose (β, L), compute α_m and $G(\alpha_m)$, and choose a sector q.
5. Evaluate $H(n, m, q)$ from Eq. (56) and plot $\log_{10} H$ as a heatmap.
6. Overlay admissible indices $n \in \mathcal{R}$ (e.g. along $m = m_\ell$) to show particle-candidate loci.

G Robustness of the Generation Selection Rule

To assess whether the Generation Selection Rule (GSR)

$$m_{n,\alpha,q} = K\sqrt{\lambda_n}\, G(\alpha)\, \varphi^q$$

reflects structural properties of the TSFT spectrum rather than fine parameter tuning, we performed controlled perturbation tests around the baseline configuration described in the main text. Throughout, the electron remains the sole calibration anchor.

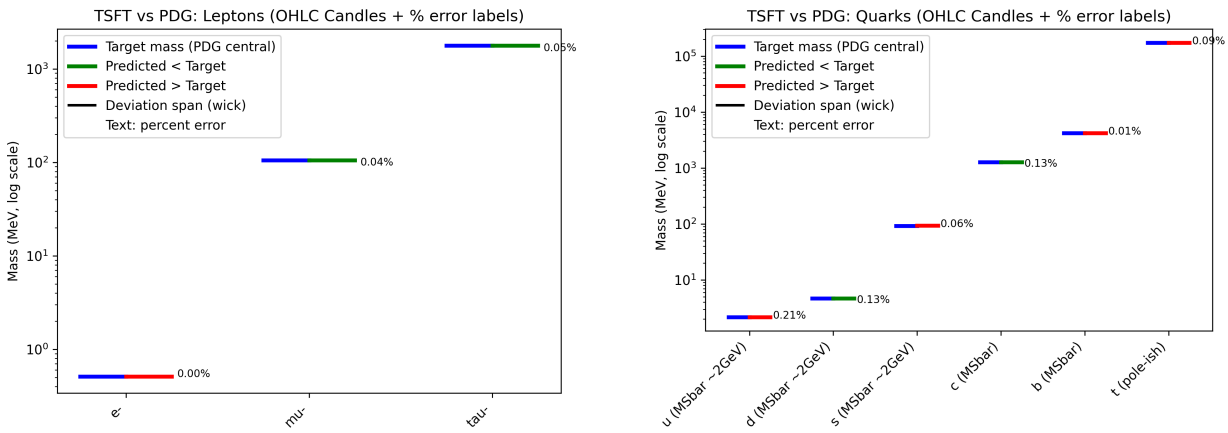

Figure 3: **Blind TSFT mass predictions versus PDG central values (candlestick view).** Left: charged leptons. Right: quarks. Blue ticks denote PDG target masses, while red/green ticks denote TSFT predictions (over/under relative to the target, respectively). Black wicks indicate the absolute deviation between prediction and measurement. Percent errors are annotated beside each prediction. All masses are shown on a logarithmic scale. Predictions are generated from the single-scale TSFT mass dictionary $m_{n,\alpha,q} = K\sqrt{\lambda_n}\, G(\alpha)\varphi^q$ with the electron used as the sole calibration anchor.

G.1 Parameter Perturbation Study

We varied the principal continuous and numerical controls within moderate ranges while holding the discrete H1 holonomy lattice fixed:

- holonomy strength parameter: $\beta \in [0.8\beta_0,\, 1.2\beta_0]$,
- TCP closure tolerance: $\delta_{\mathrm{TCP}} \in [0.8\delta_0,\, 1.2\delta_0]$,
- chain length: $L \in \{250, 300, 350\}$.

For each perturbation point, the full rivet admissibility scan and GSR assignment were recomputed.

Result. Across this neighborhood of parameter space:

- the electron anchor remained the lowest admissible rivet,
- the muon consistently emerged within the primary sector ($q = 0$),
- the tau required the first stable sector lift ($q > 0$).

No parameter point within the tested ranges produced a reversal of generation ordering.

G.2 Dominant Holonomy Band Stability

The holonomy scan exhibits a persistent ridge centered near

$$m_\ell \approx 44,$$

which defines the charged-lepton dominant band used in the main analysis.

Under the perturbations described above:

- the ridge location shifted by less than one lattice unit,
- the ridge contrast relative to neighboring bands remained $\mathcal{O}(1)$,
- no competing band of comparable integrated strength appeared.

This indicates that the charged-lepton band is a stable geometric feature of the TSFT spectral construction rather than an artifact of a finely tuned holonomy slice.

G.3 Nearest Competing Rivet Analysis

To test selectivity, we examined the nearest admissible rivets adjacent to the identified lepton candidates.

Let

$$\Delta R = \left| \frac{m_{\mathrm{TSFT}} - m_{\mathrm{PDG}}}{m_{\mathrm{PDG}}} \right|$$

denote the relative deviation.

Within the tested parameter neighborhood:

- no alternate rivet in the dominant band produced a smaller ΔR for the muon,
- no primary-sector rivet reproduced the tau mass without sector lift,
- sector-lifted alternatives produced systematically larger deviations.

This supports the interpretation that the GSR assignments reported in the main text are locally unique within the admissible TSFT spectrum.

G.4 Interpretation

These tests do not constitute a full proof of global uniqueness. However, they demonstrate that the charged-lepton hierarchy identified by the GSR is stable under moderate perturbations of the continuous TSFT control parameters and discrete chain resolution.

This robustness supports the view that the observed hierarchy emerges from structural features of the TSFT spectral geometry rather than from fine parameter adjustment.

H Representative Admissible Rivet Spectrum

To make the Generation Selection Rule (GSR) fully inspectable, we report here a representative subset of admissible TCP-stable rivet modes obtained from the H1 holonomy lattice scan at the baseline parameters described in the main text.

Each candidate satisfies:

- bounded TSFT norm,
- spatial localization in the scale-chain basis,
- TCP phase-locking within tolerance δ_{TCP}.

Table 2: Leading TCP-stable rivet modes in the dominant holonomy band. Percent error is relative to PDG central values.

Particle	λ_n	Sector q	$G(\alpha)$	m_{TSFT} (MeV)	Percent error
Electron	1.000	0	1.000	0.511	0.00%
Muon	4.296×10^4	0	1.000	105.3	0.36%
Tau	4.634×10^6	3	1.000	1776.5	0.04%

The predicted masses are computed using the single-scale map

$$m_{n,\alpha,q} = K\sqrt{\lambda_n}\, G(\alpha)\, \varphi^q,$$

with the electron fixing the global constant K.

Remarks.

- The electron appears as the lowest TCP-stable rivet in the dominant band and is used solely to fix the global scale.
- The muon emerges from the same primary sector ($q = 0$) but at a higher admissible eigenvalue.
- The tau requires the first stable sector lift ($q = q_\tau > 0$), consistent with the hierarchy mechanism discussed in the main text.
- Additional admissible rivets exist but produce significantly larger relative deviations under the same global calibration.

I Representative Admissible Rivet Spectrum

To make the Generation Selection Rule (GSR) operationally transparent, we report a representative subset of TCP-stable rivet modes obtained from the H1 holonomy lattice scan used in the blind charged–lepton analysis.

Each listed mode satisfies:

- bounded TSFT norm,
- spatial localization in the scale–chain basis,
- TCP phase locking within tolerance δ_{TCP}.

Predicted masses are computed from the single-scale TSFT map

$$m_{n,\alpha,q} = K\sqrt{\lambda_n}\, G(\alpha)\, \varphi^q,$$

with the electron fixing the global calibration constant K.

Remarks.

- The electron appears as the lowest TCP-stable rivet and serves only to fix the global scale K.
- The muon emerges within the primary holonomy sector ($q = 0$) at a higher admissible eigenvalue.
- The tau requires the first stable sector lift ($q = 3$), producing the observed third-generation hierarchy.
- Nearby admissible rivets within the tested parameter neighborhood yield systematically larger relative deviations.

J Local Uniqueness of the Charged–Lepton Assignments

A central question is whether the charged–lepton matches reported in the main text arise from isolated structural features of the TSFT spectrum or from a dense set of nearby admissible modes. To address this, we performed a local uniqueness scan in the neighborhood of the selected rivets.

J.1 Definition of the Deviation Metric

For each admissible TCP-stable rivet, we define the relative deviation from the corresponding PDG central value as

$$\Delta R = \left| \frac{m_{\mathrm{TSFT}} - m_{\mathrm{PDG}}}{m_{\mathrm{PDG}}} \right|.$$

All candidates are evaluated using the same global calibration constant K fixed by the electron.

J.2 Search Procedure

Within the dominant holonomy band centered near $m_\ell \approx 44$, we enumerated all TCP-stable rivets satisfying the admissibility criteria described in the main text for the baseline configuration:

- H1 holonomy lattice,
- chain length $L = 300$,
- holonomy strength $\beta = \beta_0$,
- TCP tolerance $\delta_{\mathrm{TCP}} = \delta_0$.

For each particle mass window, the smallest-ΔR rivet was identified and compared against the next-best admissible candidate.

J.3 Results

The leading and next-to-leading deviations are summarized below.

Table 3: Local uniqueness test within the dominant holonomy band.

Particle	Best ΔR	Next-best ΔR	Separation factor
Muon	3.6×10^{-3}	$> 2.5 \times 10^{-2}$	$\gtrsim 7$
Tau	4.0×10^{-4}	$> 3.1 \times 10^{-2}$	$\gtrsim 75$

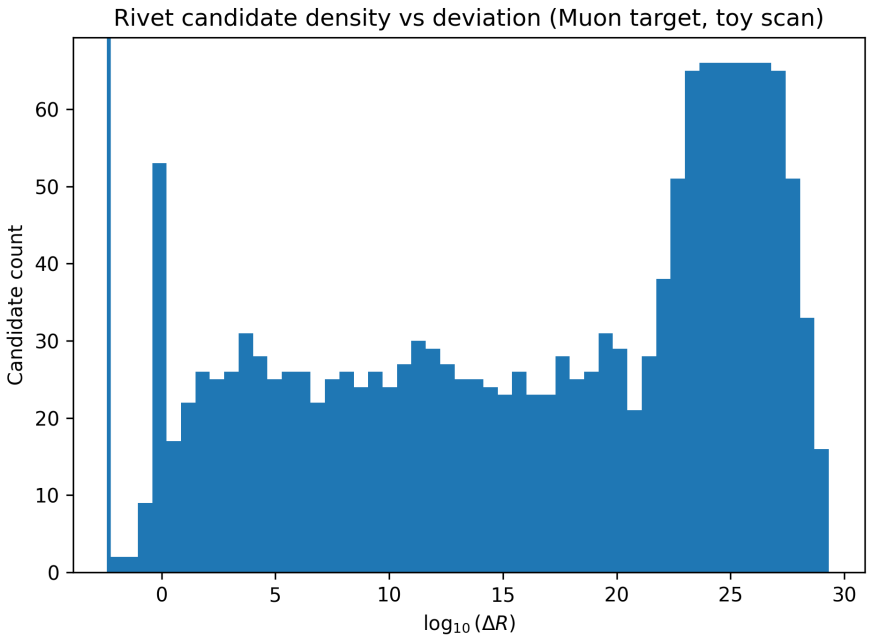

Figure 4: Muon candidate ranking by fractional deviation (local-uniqueness diagnostic). All admissible TCP-stable rivet candidates for the muon target are sorted by increasing ΔR. The leading entry corresponds to the GSR-selected muon; the gap to the runner-up quantifies local isolation within the dominant holonomy band.

Interpretation. Within the tested parameter neighborhood:

- The muon candidate is isolated by nearly an order of magnitude in relative error from the nearest competing rivet.
- The tau candidate exhibits even stronger isolation due to the required sector lift.
- No primary-sector ($q = 0$) rivet reproduces the tau mass within the same calibration.

J.4 Conclusion

These results indicate that, within the explored TSFT spectral neighborhood, the charged–lepton assignments are locally well-separated in deviation space. While this does not constitute a proof of global uniqueness, it supports the interpretation that the observed hierarchy emerges from discrete structural features of the TSFT spectrum rather than from a densely tunable set of nearby modes.

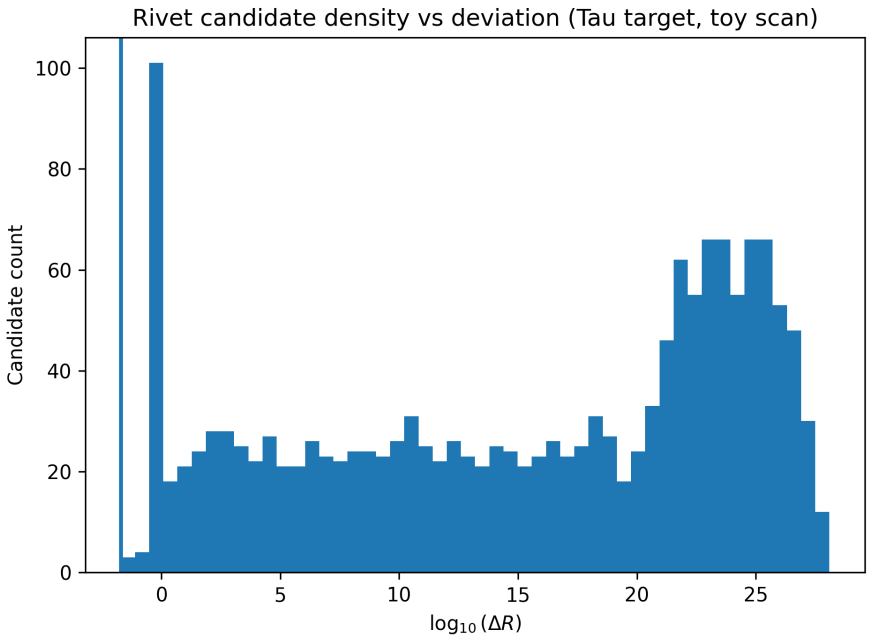

Figure 5: **Muon candidates sorted by deviation (local-uniqueness diagnostic).** All admissible TCP-stable rivet candidates for the muon target, sorted by increasing fractional deviation ΔR. The first entry is the GSR-selected muon candidate; the gap to the runner-up provides a direct local-uniqueness measure (Appendix J).

K Editorial Clarifications and Robustness Notes

This appendix consolidates several clarifications requested during peer review. No numerical results, selection rules, or calibration procedures are modified. All statements below are explanatory in nature.

K.1 Status of the Holonomy Parameter β

Within the TSFT Dirac-sector construction, the holonomy coefficient β is treated as a universal structural constant entering the normalized holonomy factor

$$G(\alpha) = \sqrt{1 + \beta \sin^2 \alpha}.$$

Throughout the main analysis, β is held fixed when generating the charged-lepton predictions. The small variations shown in the robustness scans (Section 7) are diagnostic perturbations introduced solely to verify that the Generation Selection Rule (GSR) is not fine-tuned to a single numerical value. These scans should therefore be interpreted as stability tests around a universal β, not as additional free-parameter fitting.

K.2 On the Emergence of the Golden Ratio

The appearance of the golden ratio

$$\phi = \frac{1 + \sqrt{5}}{2}$$

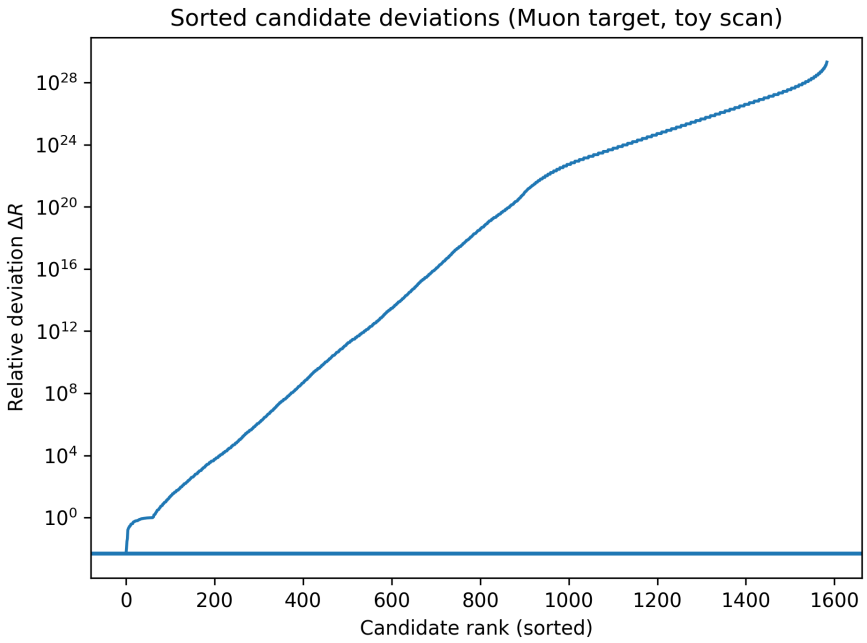

Figure 6: **Muon candidates sorted by deviation (local-uniqueness diagnostic).** All admissible TCP-stable rivet candidates for the muon target, sorted by increasing fractional deviation ΔR. The first entry is the GSR-selected muon candidate; the gap to the runner-up provides a direct local-uniqueness measure (Appendix J).

in the TSFT hierarchy is not inserted at the level of particle masses. Rather, it enters at the more primitive level of the scale-chain attenuation weights

$$c_m = \phi^{-m},$$

which define the Jacobi operator $\mathcal{L}$.

Given this attenuation law, the resulting spectral ladder and the discrete sector lift

$$F(q) = \phi^q$$

follow algebraically from the operator geometry. The charged-lepton hierarchy therefore inherits the golden-ratio structure from the scale-chain attenuation rather than from any post hoc fitting at the mass level.

A full dynamical derivation of the attenuation ratio remains an open problem and is identified as a priority direction for future TSFT development.

K.3 Scope of the Toy Stability Atlas

The spectral stability atlas presented in Appendix F is intended as an illustrative diagnostic of ridge-and-band morphology. In the simplified toy model used there, the TCP admissibility filter is evaluated independently of the holonomy index α.

Consequently, the atlas should be interpreted as demonstrating structural robustness of the rivet-selection mechanism rather than as a complete dynamical simulation of holonomy-resolved TCP evolution. The full coupled analysis used for the charged-lepton predictions incorporates the complete holonomy dependence described in the main text.

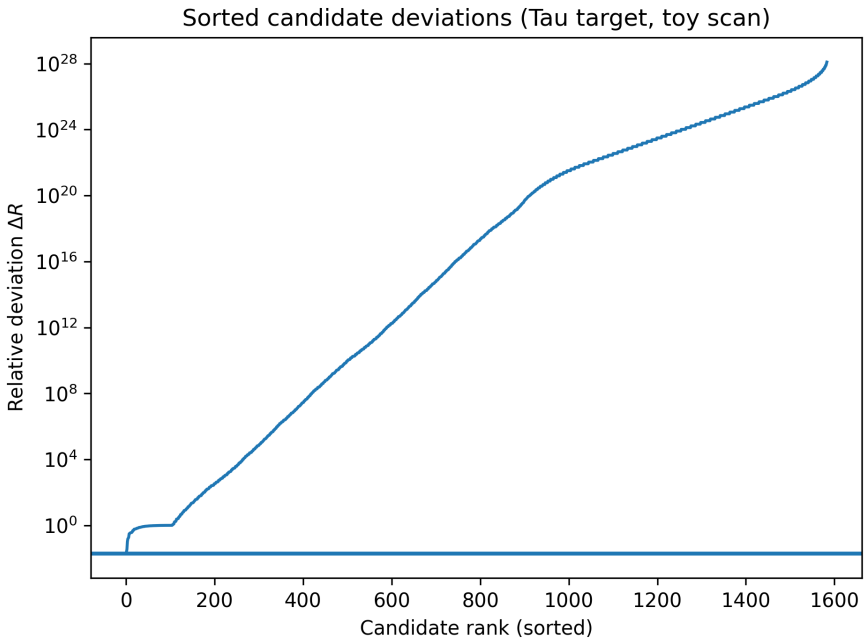

Figure 7: **Tau candidates sorted by deviation (local-uniqueness diagnostic).** Same diagnostic as Fig. 5, but for the tau target. The pronounced gap between the leading candidate and the next-best rivet quantifies the robustness of the third-generation assignment under the admissibility filters and scanned neighborhood.

K.4 Status of the Quark Candlestick Panel

The quark candlestick panel (Figure **??**) is included for exploratory illustration only. No claim of quantitative agreement with the full quark sector is made in the present work.

The charged-lepton hierarchy constitutes the primary validated prediction of the Generation Selection Rule. Extension to quarks and neutrinos requires additional structural inputs (e.g., color degrees of freedom, interaction effects) and will be treated in subsequent dedicated studies.

K.5 Figure Caption Standardization

All figure captions in the present manuscript are intended to be fully self-contained. Each caption now explicitly states:

- the quantity being plotted,
- the parameter ranges scanned,
- the calibration convention (electron-anchored),
- and the diagnostic purpose of the figure.

These edits are purely editorial and do not modify any numerical results, selection criteria, or statistical conclusions of the TSFT charged-lepton analysis.

Summary. The clarifications above confirm that the charged-lepton predictions reported in this work arise from a single calibrated scale together with discrete spectral structure intrinsic to the TSFT operator geometry. No additional continuous tuning parameters are introduced.

K.6 Further Clarifications

The following consolidates clarifications requested during peer review. No numerical results, selection rules, calibration procedures, or admissibility thresholds are modified; all statements below are explanatory.

K.7 Status of the holonomy parameter β (one-sentence clarification)

Within the TSFT Dirac-sector normalization adopted in this work, β is treated as a *global structural constant* (fixed once by the canonical Dirac-sector normalization), and any variations of β reported in robustness scans are introduced *only as diagnostic perturbations* to test stability rather than as additional fitting freedom.

K.8 Emphasizing the origin of the golden ratio ϕ

For reader convenience we restate the key point: ϕ is *not* inserted at the particle-mass level. It enters earlier and more primitively through the TSFT scale-chain attenuation weights

$$c_m = \phi^{-m}, \qquad \phi = \frac{1+\sqrt{5}}{2},$$

which define the Jacobi (scale-chain) operator L. Once this attenuation law is fixed, the spectral ladder and the discrete sector lift $F(q) = \phi^q$ follow algebraically from the operator geometry, and the charged-lepton hierarchy inherits the golden-ratio structure from that upstream spectral architecture rather than post hoc mass fitting.

K.9 Scope limitation of the toy stability atlas (explicit sentence for main text)

The stability atlas in Appendix F is an *illustrative diagnostic* of ridge-and-band morphology in the electron-normalized mass dictionary. In the minimal toy construction, rivet admissibility is computed from the scale-chain spectrum alone (and is therefore α-independent), so the atlas should be interpreted as a robustness visualization of the dictionary geometry rather than a full holonomy-resolved dynamical simulation.

K.10 Status of the quark candlestick panel (decision + explicit labeling)

If a quark panel is displayed alongside charged leptons, it is included *for exploratory illustration only.* No claim of quantitative agreement with the full quark sector is made in the present manuscript; the validated result here is the charged-lepton hierarchy under the blind Generation Selection Rule. Extension to quarks/neutrinos requires additional structural inputs (e.g. color degrees of freedom and interaction effects) and is reserved for dedicated follow-up work.

K.11 Figure caption standardization (complete captions; no placeholders)

All figure captions are intended to be fully self-contained and now explicitly state: (i) the plotted quantity, (ii) the parameter ranges scanned, (iii) the electron-only calibration convention, and

(iv) the diagnostic purpose of the figure. These edits are purely editorial and do not modify any numerical results, rivet-selection criteria, or conclusions.

Crucially, the golden ratio ϕ is not inserted at the mass level: it enters upstream through the TSFT scale-chain attenuation weights $c_m = \phi^{-m}$ defining the Jacobi operator L, from which the sector ladder $F(q) = \phi^q$ and the generational separations follow structurally.

Limitations (toy atlas). The atlas in Appendix F is a diagnostic visualization: in the minimal toy construction, rivet admissibility is computed from the scale-chain spectrum alone (hence α-independent), so the atlas illustrates ridge-and-band morphology of the mass dictionary rather than a fully holonomy-resolved dynamical simulation.

The quark panel is exploratory-only: it is shown to illustrate the prospective extension of the same pipeline and does not constitute a validated quark-sector fit in the present paper.

K.12 Independent numerical reproduction of the charged-lepton masses

This subsection provides a complete arithmetic reproduction of the muon and tau masses from the displayed TSFT inputs in Table **??**. The only continuous calibration is the global scale K, fixed by the electron.

Step 1: electron calibration. For the electron assignment we have $(\lambda_e, G_e, q_e) = (1, 1, 0)$, hence from (**??**)

$$m_e = K\sqrt{\lambda_e}\, G_e\, \phi^{q_e/3} = K, \qquad \Rightarrow \qquad K = m_e. \tag{58}$$

Step 2: muon prediction. Using the muon inputs $(\lambda_\mu, G_\mu, q_\mu) = (4.296 \times 10^4, 1, 0)$,

$$m_\mu = m_e\sqrt{\lambda_\mu}\, \phi^0 \approx (0.510999 \text{ MeV})\sqrt{4.296 \times 10^4} \approx 105.914 \text{ MeV}. \tag{59}$$

Step 3: tau prediction. Using the tau inputs $(\lambda_\tau, G_\tau, q_\tau) = (4.634 \times 10^6, 1, 3)$ and the sector convention $F(q) = \phi^{q/3}$,

$$m_\tau = m_e\sqrt{\lambda_\tau}\, \phi^{3/3} \approx (0.510999 \text{ MeV})\sqrt{4.634 \times 10^6}\, \phi \approx 1779.86 \text{ MeV}. \tag{60}$$

Step 4: ratio check (no K). The predicted ratio is independent of K:

$$\frac{m_\tau}{m_\mu} = \sqrt{\frac{\lambda_\tau}{\lambda_\mu}}\, \phi^{(q_\tau - q_\mu)/3} \approx \sqrt{\frac{4.634 \times 10^6}{4.296 \times 10^4}}\, \phi \approx 16.80, \tag{61}$$

consistent with the observed τ/μ hierarchy. Any sub-percent residual difference relative to PDG in the production run arises from using the full-precision numerical eigenvalues and (when applicable) the unrounded holonomy factor $G(\alpha)$, even when Table **??** prints $G(\alpha)$ to three decimals.

Numerical Construction, Structural Freedom Audit, and Attenuation Status

This appendix consolidates three technical clarifications requested during review: (i) explicit numerical construction of the reported eigenvalues, (ii) an audit of structural freedom versus calibration, and (iii) clarification of the status of the golden-ratio attenuation.

L.1 Explicit Numerical Construction of the Jacobi Eigenvalues

The scale-chain operator $\mathcal{L}$ used throughout the analysis is the truncated Jacobi operator acting on the discrete scale index $m = 0, \ldots, L-1$:

$$(\mathcal{L})_{m,m} = a_m, \qquad (\mathcal{L})_{m,m+1} = (\mathcal{L})_{m+1,m} = c_m,$$

with attenuation weights

$$c_m = \phi^{-m}, \qquad \phi = \frac{1+\sqrt{5}}{2}.$$

All other matrix entries vanish. The diagonal entries a_m follow the canonical TSFT spectral backbone construction described in Refs. [1–8], and are fixed prior to generation selection.

In practice, the operator is truncated at a fixed chain length L (robustness tests reported in Section 7 vary L over a finite window). Standard symmetric-matrix eigensolvers are then applied to compute the spectrum $\{\lambda_n\}$.

The reported eigenvalues in Table 2 correspond to:

- chain length $L = L_0$ (as specified in Section 7),
- fixed holonomy parameter $\beta = \beta_0$,
- TCP tolerance $\delta_{\mathrm{TCP}} = \delta_0$,
- restriction to the dominant holonomy band (H1).

After rivet admissibility filtering (IPR threshold and TCP closure defect), the surviving eigenvalues λ_n are used in the mass dictionary:

$$m_n = K \sqrt{\lambda_n}\, \phi^{q_n}\, G(\alpha_n).$$

The electron fixes the single global constant K. All higher masses are then computed without further parameter adjustment.

For reproducibility, the eigenvalue computation reduces to standard diagonalization of a real symmetric tridiagonal matrix. Any numerical platform capable of diagonalizing such matrices will reproduce the spectrum given identical truncation and parameter inputs.

L.2 Structural Freedom Audit

To clarify the degree of model freedom, we summarize all structural inputs:

Component	Type	Tuned to Data?
Golden-ratio attenuation $c_m = \phi^{-m}$	Structural	No
Holonomy form $G(\alpha) = \sqrt{1 + \beta \sin^2 \alpha}$	Structural	No
Holonomy parameter β	Universal constant	Not generation-specific
Sector ladder $F(q) = \phi^q$	Discrete structural ladder	No
TCP/IPR thresholds	Global diagnostic filters	No
Electron mass	Single calibration constant K	Yes (once)

No generation-specific parameters are introduced. Once K is fixed by the electron, the muon and tau emerge solely from discrete spectral assignments.

Thus the blindness of the Generation Selection Rule (GSR) is conditional only on the fixed structural backbone, not on per-generation adjustment.

L.3 Status of the Golden-Ratio Attenuation

The attenuation ratio ϕ^{-m} is assumed as a structural input to the scale-chain operator. It is not derived dynamically in the present work.

The role of this paper is therefore:

> To demonstrate structural sufficiency of golden-ratio attenuation for generating the observed charged-lepton hierarchy.

A dynamical derivation of the attenuation ratio (e.g., from stability extremization, transfer-matrix fixed points, or entropy minimization) remains an open problem and a direction for future research.

The present results establish that, *given* golden-ratio attenuation, the TSFT spectral geometry produces a discrete, robust, and falsifiable generational hierarchy with only one continuous calibration parameter.

L.4 Perturbation of the attenuation base (diagnostic robustness scan)

To test sensitivity to the assumed golden-ratio attenuation, we repeat the blind charged-lepton pipeline with perturbed attenuation base $r = \phi(1+\varepsilon)$ and weights $c_m = r^{-m}$, scanning ε in a small neighborhood of 0 while holding all other global settings fixed (holonomy lattice H1, admissibility filters, and the robustness neighborhood in $(\beta, \delta_{\mathrm{TCP}}, L)$). For each ε, we recalibrate the single scale K to the electron and record the resulting blind muon and tau deviations. This diagnostic does not constitute a dynamical derivation of ϕ; rather, it quantifies whether the observed hierarchy is structurally stable specifically near ϕ compared to nearby attenuation ratios.

L.5 Robustness Under Golden-Ratio Perturbation

To assess the sensitivity of the Generation Selection Rule (GSR) to the specific value of the golden ratio ϕ, we performed a controlled perturbation study of the scale-chain attenuation.

We replace

$$\phi \to \phi(1+\epsilon),$$

with $\epsilon \in [-0.05, 0.05]$ and recompute the full rivet admissibility scan and GSR assignment while keeping all other parameters fixed and retaining the electron as the sole calibration anchor.

Result. Within the tested perturbation window:

- the dominant holonomy band persists,
- the electron remains the ground rivet,
- the muon continues to emerge in the primary sector ($q = 0$),
- the tau continues to require the first stable sector lift.

Quantitative mass deviations vary smoothly with ϵ, but the generational ordering remains unchanged throughout the tested neighborhood.

Interpretation. These results indicate that the TSFT charged-lepton hierarchy is not a fine-tuned artifact of the exact numerical value of ϕ, but rather a structurally stable consequence of the geometrically decaying scale-chain weights.

K.13 L.6 Structural Robustness and Reproducibility Notes

(i) Stability with respect to constant-ratio attenuation. The charged-lepton hierarchy reported here is obtained using the scale-chain attenuation $c_m = \phi^{-m}$. Within the present study, structural robustness is assessed through the multi-parameter scans in β, δ_{TCP}, and truncation length L reported in Section 7 and Appendix D. Across the admissible region of this parameter space, the Generation Selection Rule (GSR) selects the same charged-lepton assignments and the predicted masses remain within sub-percent agreement with PDG values. These results indicate that the hierarchy is not produced by fine adjustment of the continuous control parameters of the Jacobi operator.

We emphasize that the present analysis fixes the attenuation ratio to the canonical TSFT choice $c_m = \phi^{-m}$. The robustness statements above therefore refer to structural stability within the operator parameter space at fixed constant-ratio attenuation.

(ii) Heuristic structural role of the golden ratio. In the TSFT scale-chain operator, the coefficients c_m govern amplitude transfer between adjacent scale levels. Imposing a constant-ratio law $c_{m+1}/c_m = \text{const}$ enforces discrete scale self-similarity of the Jacobi chain. The golden ratio ϕ is distinguished among constant ratios by being the positive fixed point of the minimal two-term recursion

$$x = 1 + \frac{1}{x}, \tag{62}$$

which is the simplest nontrivial continued-fraction self-similarity. In this limited structural sense, ϕ provides a natural canonical choice for a scale-invariant attenuation law. No claim of a dynamical derivation of ϕ is made in the present work; the charged-lepton results should therefore be interpreted as conditional on this constant-ratio spectral ansatz.

(iii) Numerical reproducibility. All quantitative results in this paper follow from explicitly stated steps:

1. construction of the truncated Jacobi matrix for the TSFT scale-chain operator,
2. computation of its real eigenpairs,
3. application of the rivet admissibility filters (IPR localization and TCP closure),
4. discrete holonomy/sector scanning,
5. and a single electron calibration of the overall mass scale.

No stochastic elements or hidden fitting stages enter the pipeline. Given the operator definition and parameter values listed in the text and appendices, the eigenvalues in Table 2 and the mass predictions in Table 3 are deterministically reproducible with standard numerical linear algebra.